Supporting Information

A multifunctional selective "turn-on" fluorescent chemosensor for detection of Group IIIA ions Al^{3+}, Ga^{3+} and In^{3+}

Hyo Jung Jang, Ji Hye Kang, Dongju Yun, Cheal Kim*

Depart. of Fine Chem., Seoul National Univ. of Sci. and Tech., Seoul 139-742*, Korea.*
Fax: +82-2-973-9140; Tel: +82-2-970-6681; E-mail: chealkim@seoultech.ac.kr

The method of determination of association constant (*K*). Based on the literatures [1,2], the association constant (*K*) of sensor **1** (L) with Al^{3+}, Ga^{3+} and In^{3+} (M) can be expressed by the following equations, where (L) and (M) are assumed to form a complex with a complexation ratio of m:n.

$$[M]^m = \frac{1}{nK}\frac{1}{[L]_T^{n-1}}\frac{1-\alpha}{\alpha^n}, \quad \alpha = \frac{[L]}{[L]_T}$$

α is defined as the ratio between the free ligand concentration [L] and the initial concentration of ligand $[L]_T$.

References

[1] C.-Y. Li, X.-B. Zhang, Y.-Y. Dong, Q.-J. Ma, Z.-X. Han, Y. Zhao, G.-L. Shen and R.-Q. Yu, A porphyrin derivative containing 2-(oxymethyl)pyridine units showing unexpected ratiometric fluorescent recognition of Zn^{2+} with high selectivity, Anal. Chim. Acta., 2008, **616**, 214-221.

[2] G. Grynkiewicz, M. Poenie and R.Y. Tsien, A new generation of Ca^{2+} indicators with greatly improved fluorescence properties, J. Biol. Chem., 1985, **260**, 3440-3450.

Table S1. Examples for the detection of In^{3+} by organic chemosensors.

Sensor	Detection limit (μM)	Binding constant	Water % in solvent	Method of detection	Reference
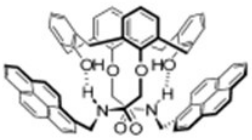	No data	7.4×10^3	0%	Fluorescence	[1]
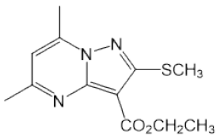	0.19	No data	0%	Fluorescence	[2]
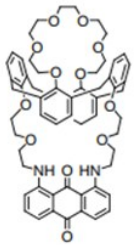	No data	No data	0%	Fluorescence	[3]
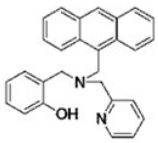	2	1.4×10^5	0%	Fluorescence	[4]
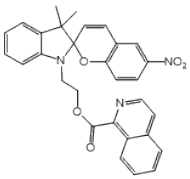	10	No data	50%	Fluorescence Naked eye	[5]
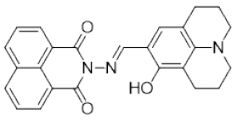	7.92	1.0×10^8	0%	Fluoresecnce	this work

References

[1] S.K. Kim, S.H. Kim, H.J. Kim, S.H. Lee, S.W. Lee, J. Ko, R.A. Bartsch and J.S. Kim, Indium(III)-Induced Fluorescent Excimer Formation and Extinction in Calix[4]arene−Fluoroionophores, Inorg. Chem., 2005, **44**, 7866–7875.

[2] Y.-C. Wu, H.-J. Li and H.-Z. Yang, A sensitive and highly selective fluorescent sensor for In(3+), Org. Biomol. Chem., 2010, **8**, 3394–3397.

[3] D.Y. Han, J.M. Kim, J. Kim, H.S. Jung, Y.H. Lee, J.F. Zhang and J.S. Kim, ESIPT-based anthraquinonylcalix[4]crown chemosensor for In^{3+}, Tetrahedron Lett., 2010, **51**, 1947–1951.

[4] H. Kim, K.B. Kim, E.J. Song, I.H. Hwang, J.Y. Noh, P.G. Kim, K.D. Jeong and C. Kim, Turn-on selective fluorescent probe for trivalent cations, Inorg. Chem. Commun., 2013, **36**, 72–76.

[5] Y.-M. Kho and E. Shin, Spiropyran-Isoquinoline Dyad as a Dual Chemosensor for Co(II) and In(III) Detection, Molecules, 2017, **22**, 1569–1582.

(a)

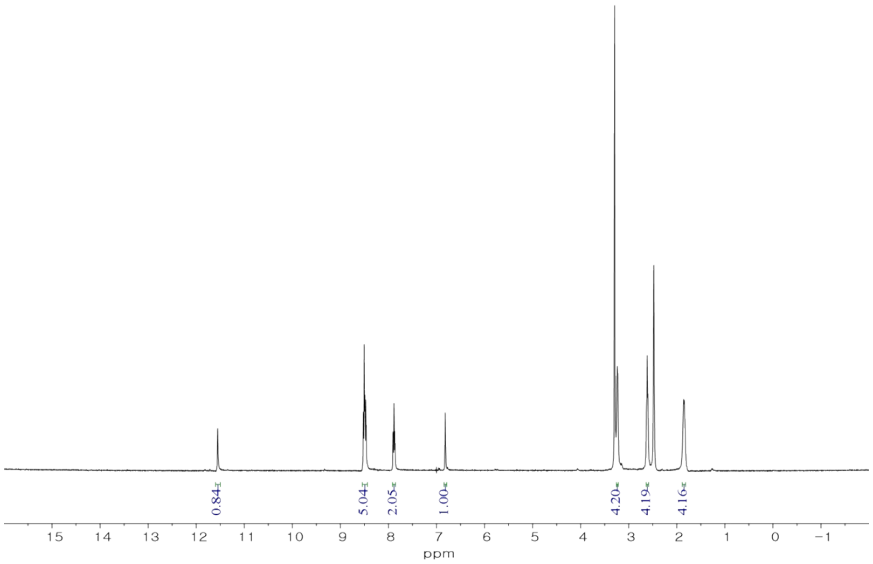

(b)

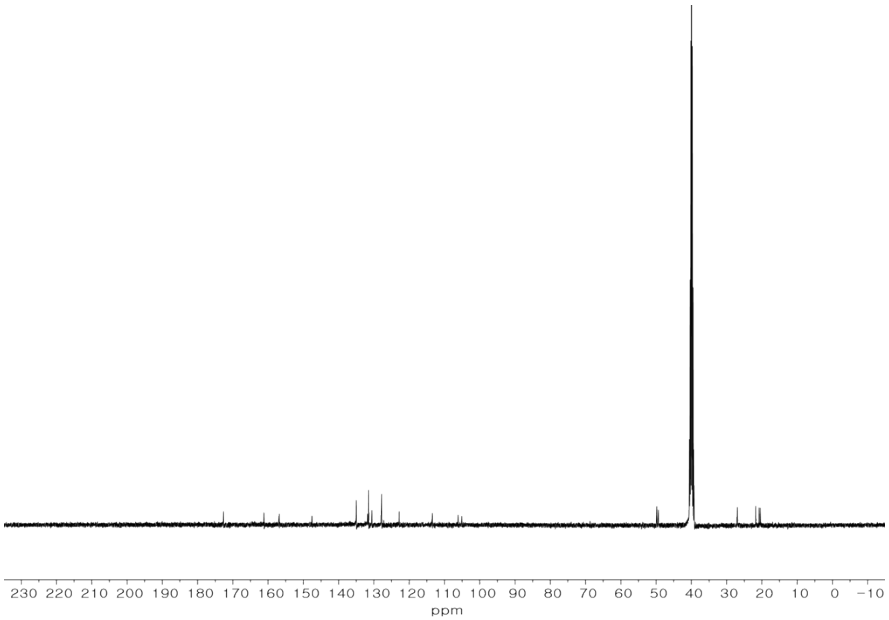

Fig. S1 (a) ^{1}H NMR and (b) ^{13}C NMR spectra of **1**.

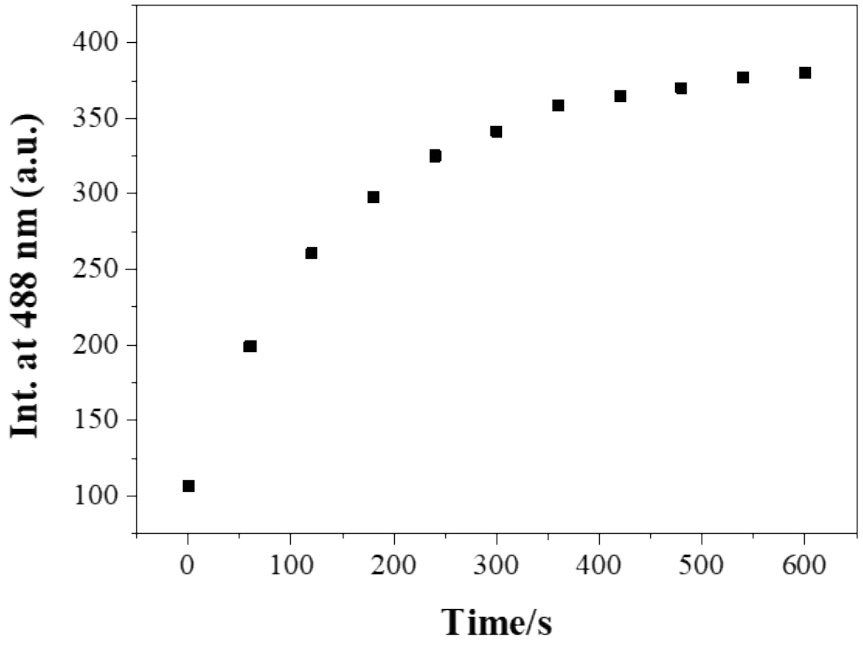

Fig. S2 Time-dependent fluorescence intensity changes of **1** (20 μM) in the presence of Al^{3+} in MeOH with excitation at 368 nm.

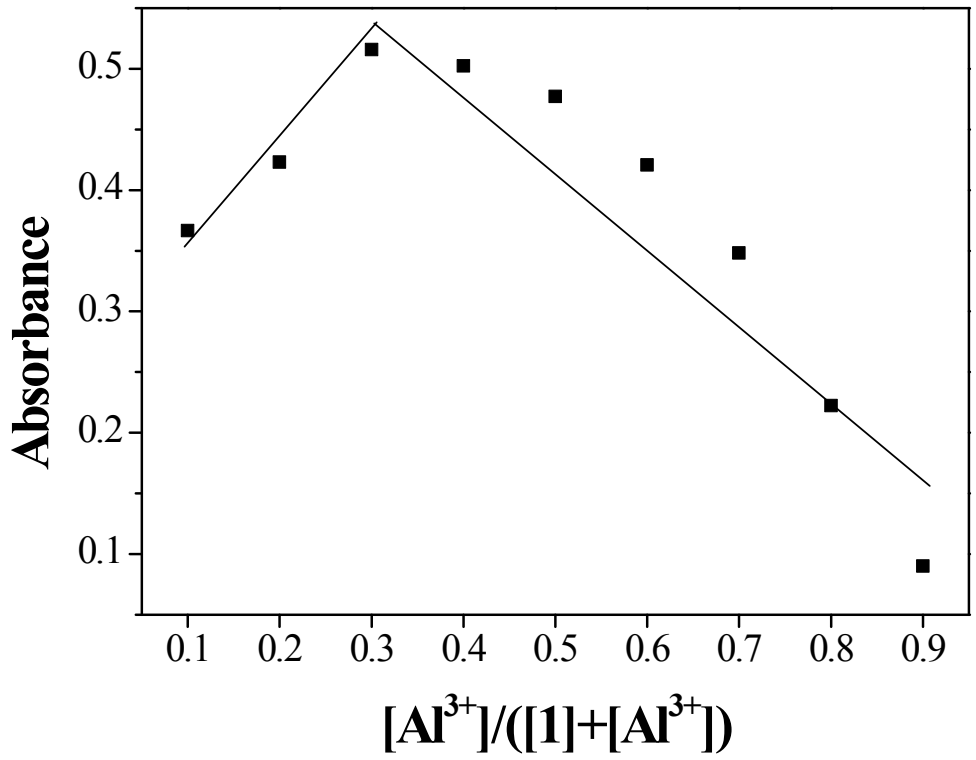

Fig. S3 Job plot of **1** and Al^{3+}. The total concentration of **1** and Al^{3+} was 20 μM.

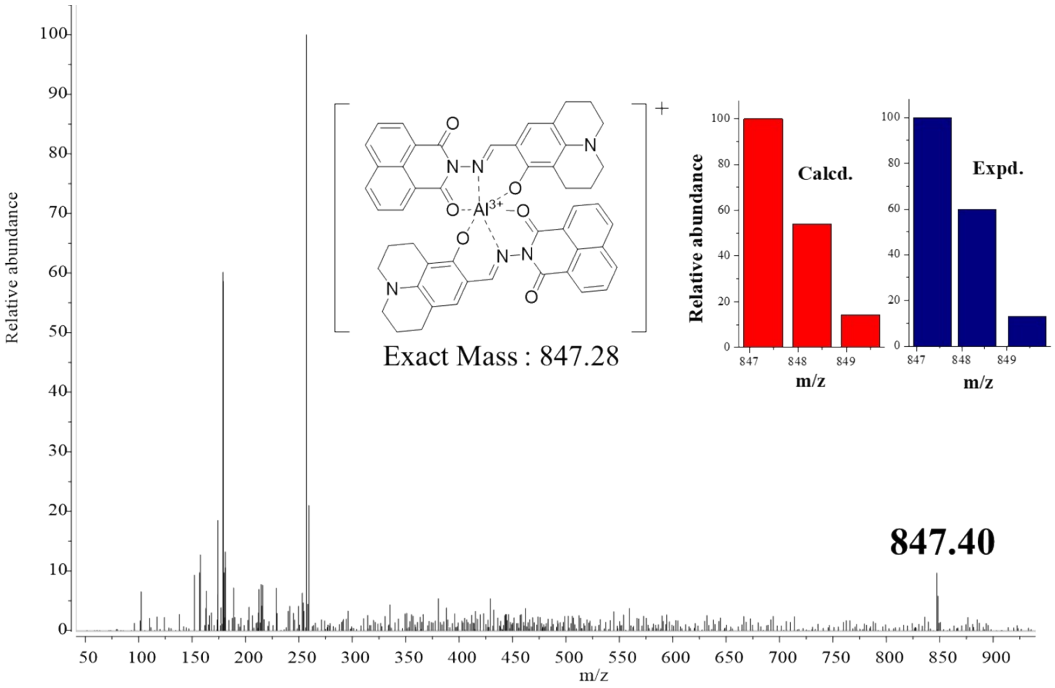

Fig. S4 Positive-ion electrospray ionization mass spectrum of **1** (100 μM) upon addition of 1.0 equiv of $Al(NO_3)_3$.

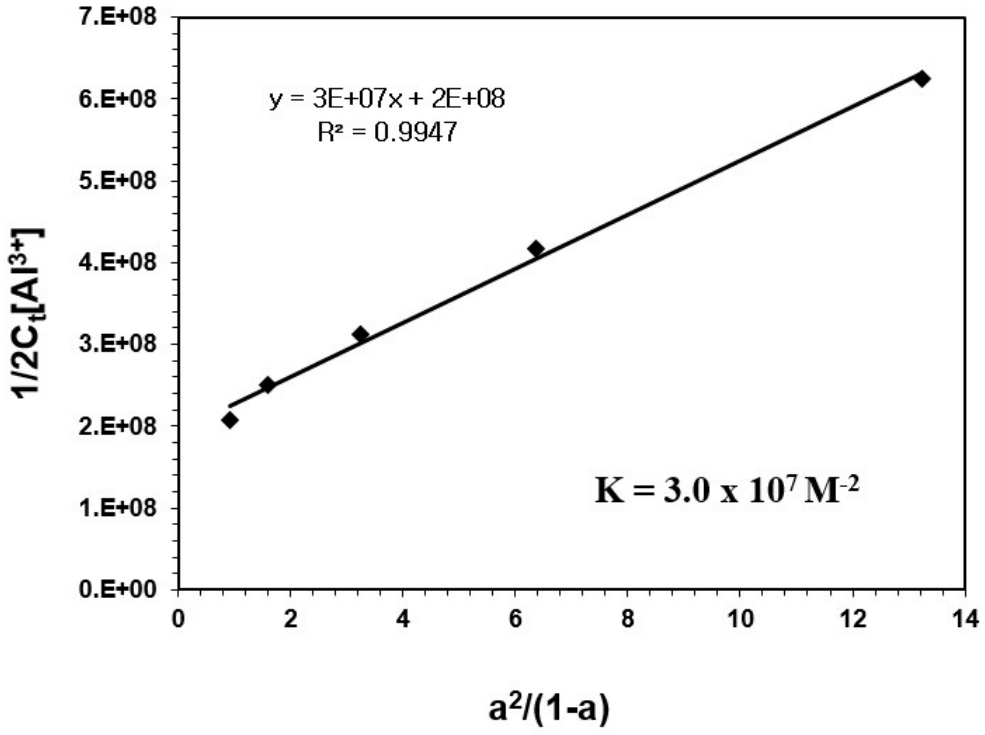

Fig. S5 Li's equation of **1** (20 μM) for Al^{3+}, assuming 2:1 stoichiometry for association of **1** with Al^{3+}.

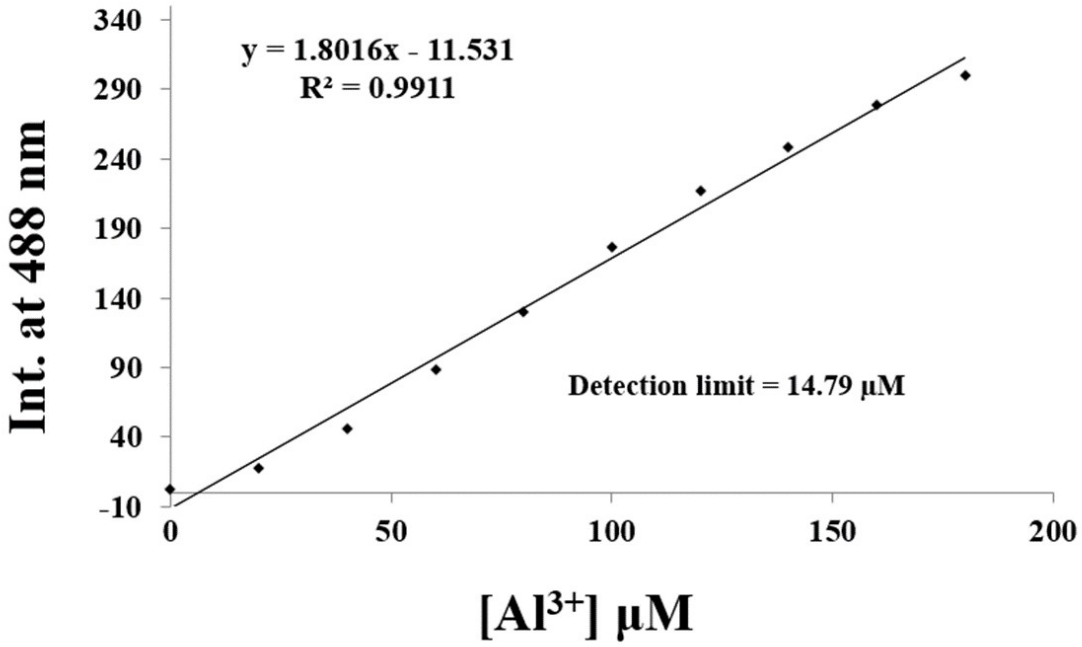

Fig. S6 Detection limit of **1** (20 μM) for Al^{3+} through change of fluorescence intensity.

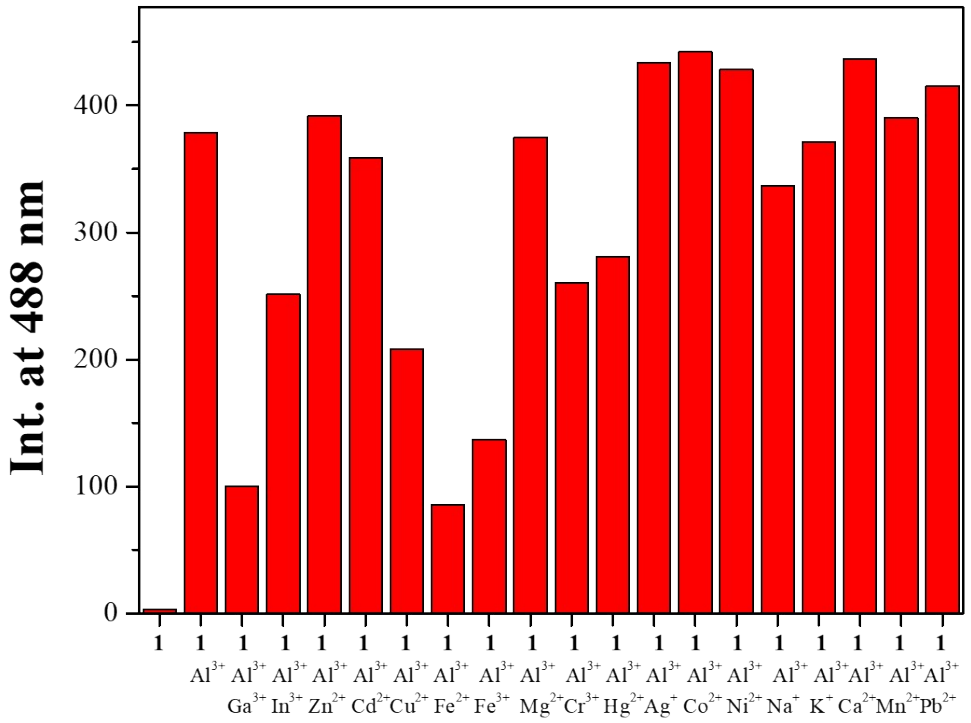

Fig. S7 Competitive selectivity of **1** (20 μM) toward Al^{3+} (22 equiv) in the presence of other metal ions (22 equiv).

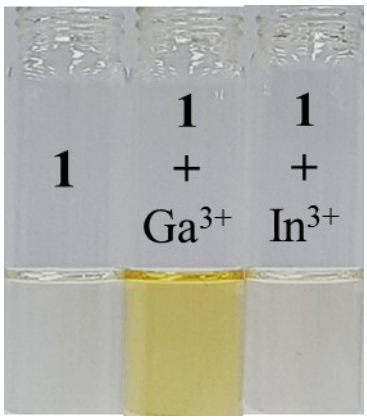

Fig. S8 Color changes of **1**, Ga^{3+}-2·**1** and In^{3+}-2·**1**.

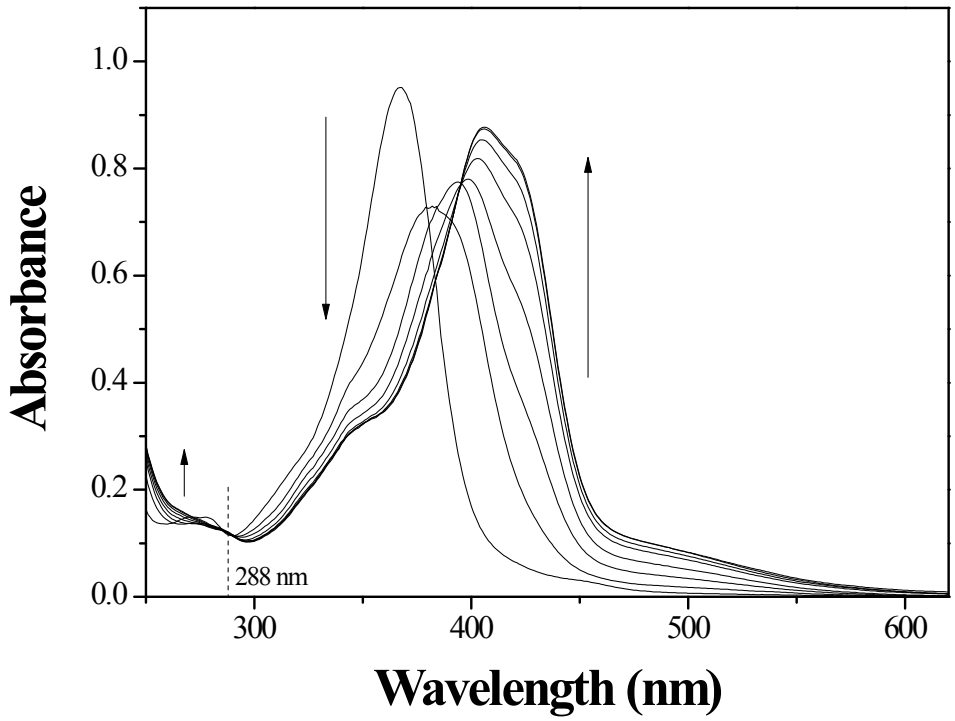

Fig. S9 UV-vis spectral changes of **1** (20 μM) in the presence of different concentrations of Ga^{3+} ion.

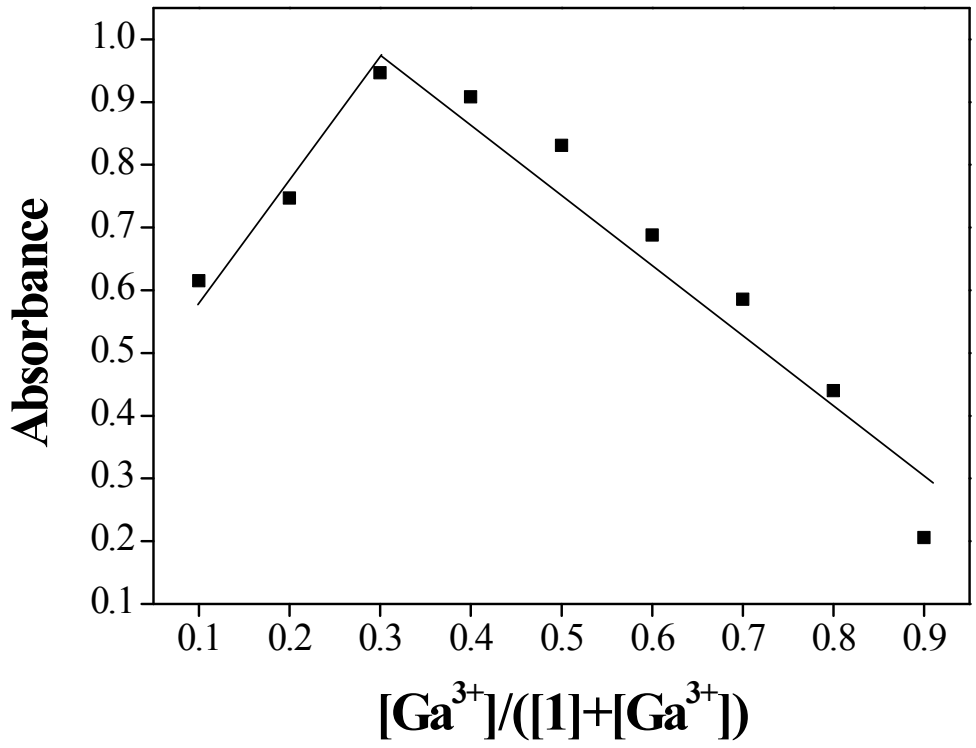

Fig. S10 Job plot of **1** and Ga^{3+}. The total concentration of **1** and Ga^{3+} was 20 μM.

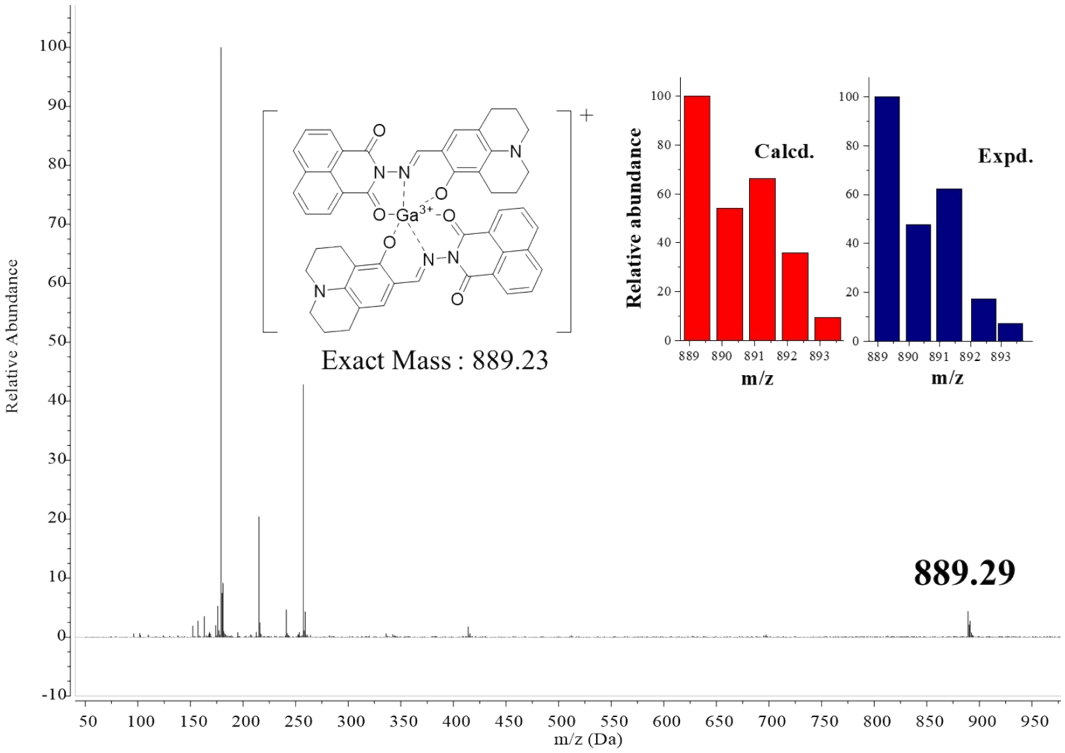

Fig. S11 Positive-ion electrospray ionization mass spectrum of **1** (100 μM) upon addition of 1.0 equiv of $Ga(NO_3)_3$.

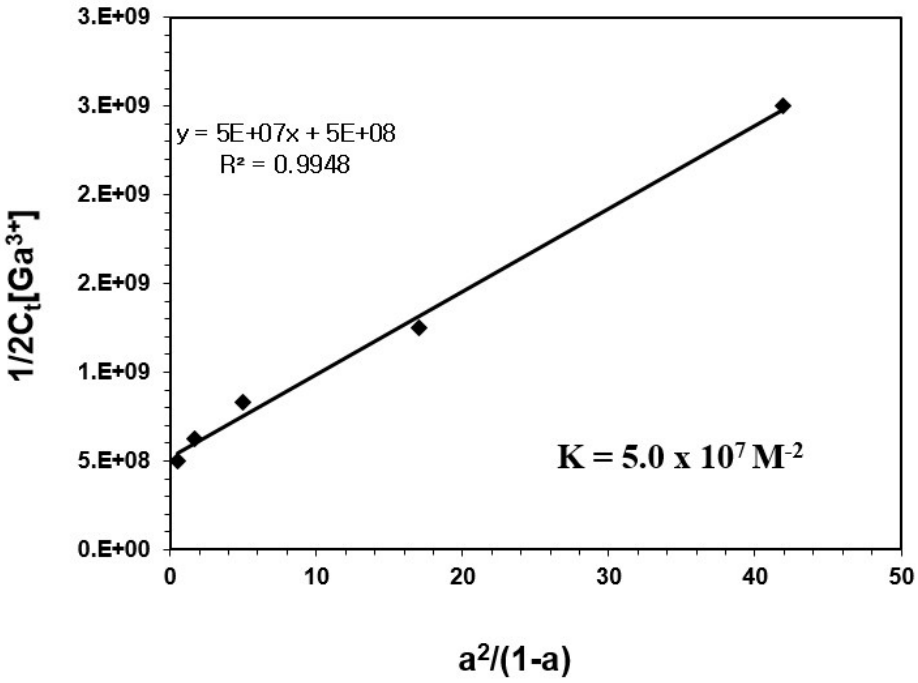

Fig. S12 Li's equation of **1** (20 μM) for Ga^{3+}, assuming 2:1 stoichiometry for association of **1** with Ga^{3+}.

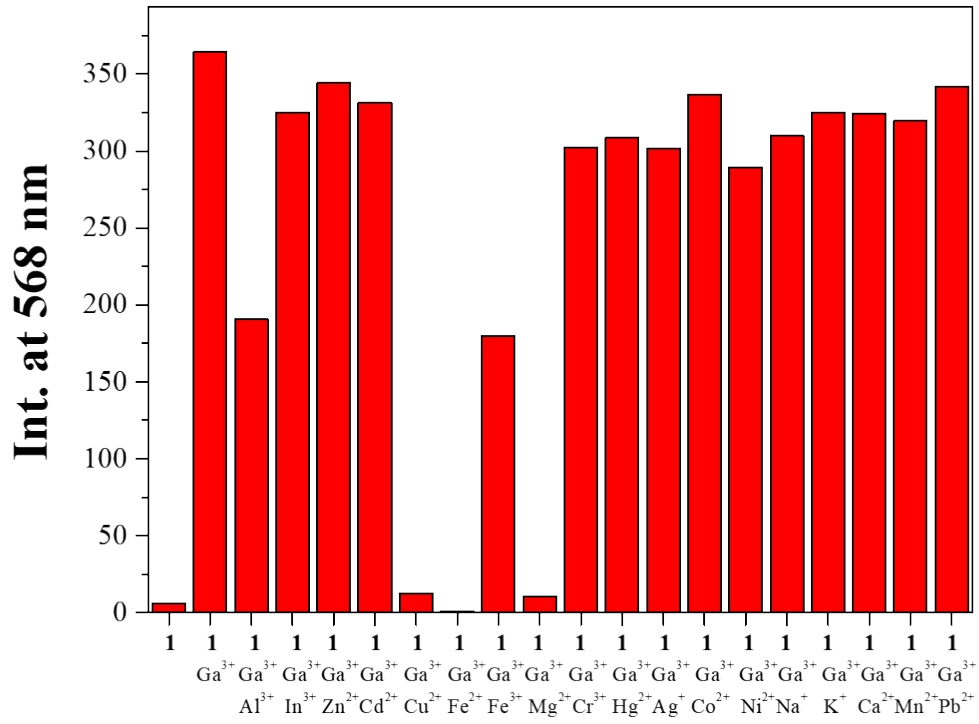

Fig. S13 Competitive selectivity of **1** (20 μM) toward Ga^{3+} (9 equiv) in the presence of other metal ions (9 equiv).

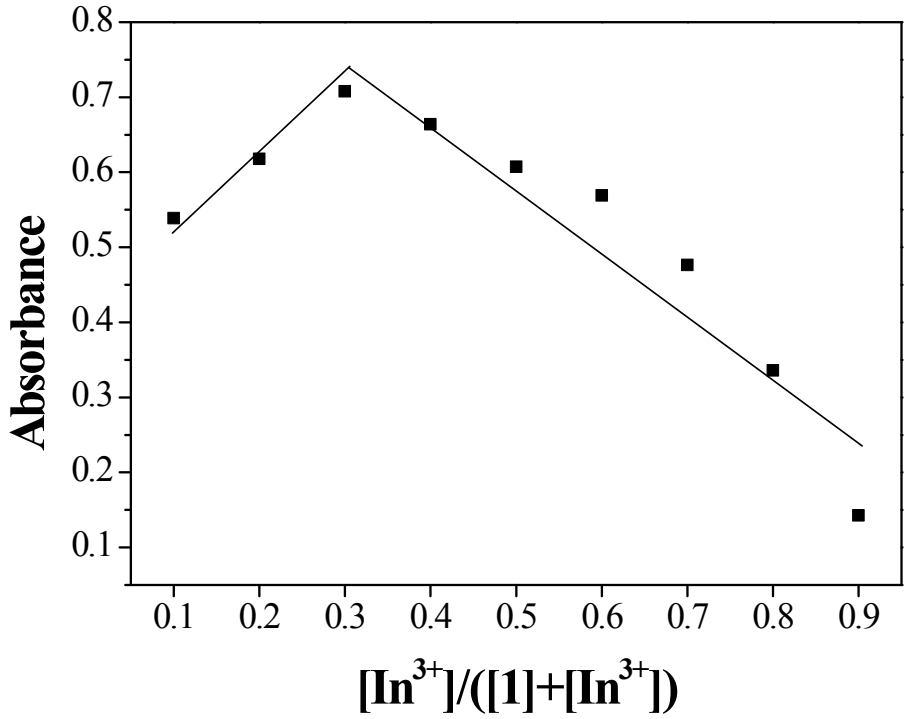

Fig. S14 Job plot of **1** and In^{3+}. The total concentration of **1** and In^{3+} was 20 μM.

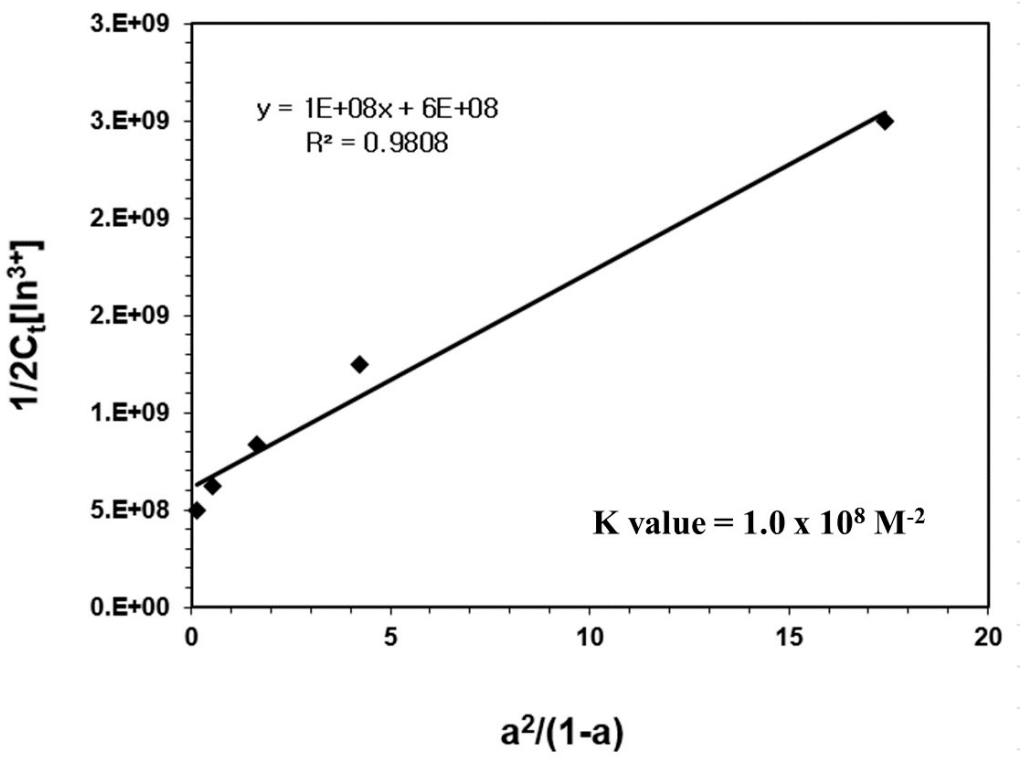

Fig. S15 Li's equation of **1** (20 μM) for In^{3+}, assuming 2:1 stoichiometry for association of **1** with In^{3+}.

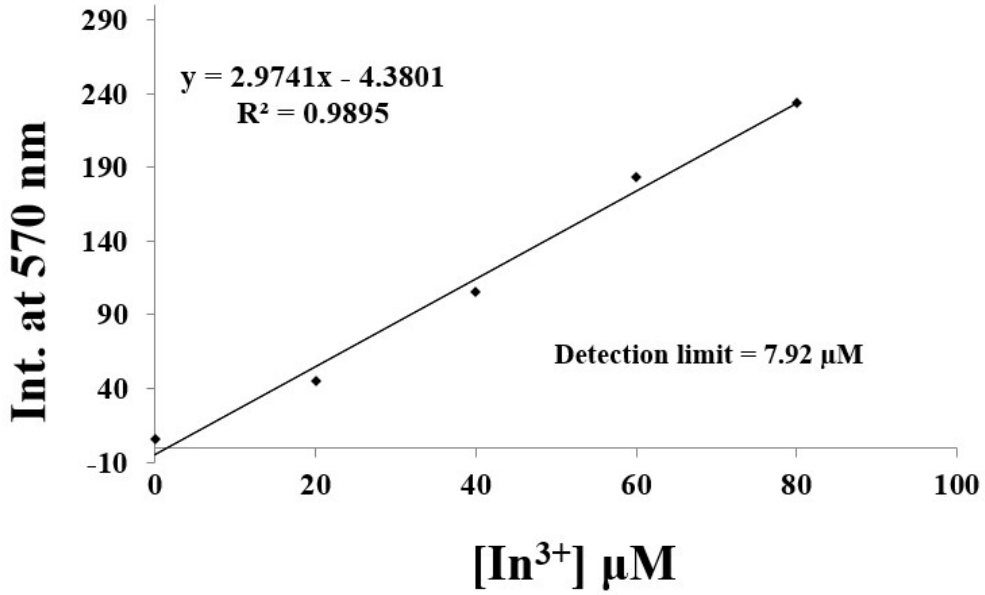

Fig. S16 Detection limit of **1** (20 µM) for In^{3+} through change of fluorescence intensity.

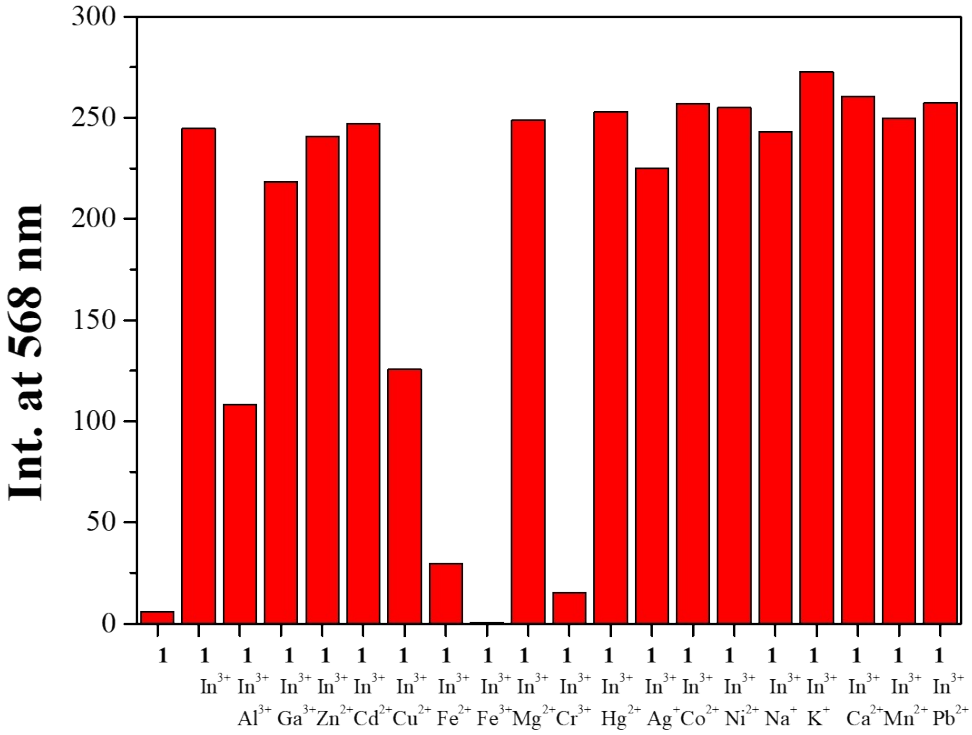

Fig. S17 Competitive selectivity of **1** (20 μM) toward In^{3+} (9 equiv) in the presence of other metal ions (9 equiv).

(a)

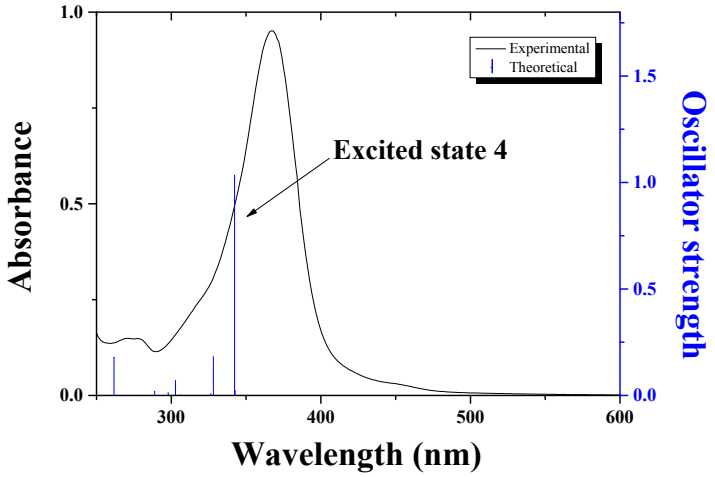

(b)

Excited state 4	Wavelength (nm)	Percent (%)	Main character	Oscillator strength
H-2 → L	342.30	60	π → π*	1.0340
H → L+1		37		

Fig. S18 (a) The theoretical excitation energies (TD-DFT method) and the experimental UV-vis spectrum of **1**. (b) The major electronic transition energies and molecular orbital contributions of **1** (H = HOMO and L = LUMO).

(a)

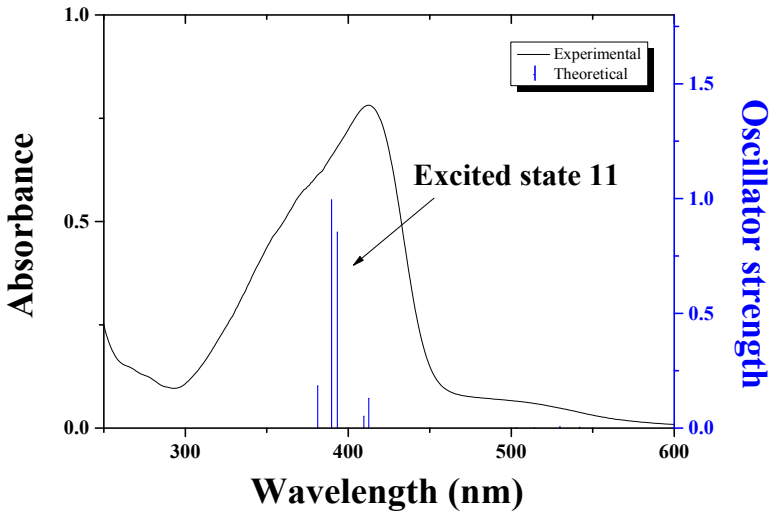

(b)

Excited state 11	Wavelength (nm)	Percent (%)	Main character	Oscillator strength
H → L+2	393.28	13	ICT	0.8534
H → L+3		66	ICT	

Fig. S19 (a) The theoretical excitation energies (TD-DFT method) and the experimental UV-vis spectrum of Al^{3+}-2·**1** complex. (b) The major electronic transition energies and molecular orbital contributions of Al^{3+}-2·**1** complex (H = HOMO and L = LUMO).

(a)

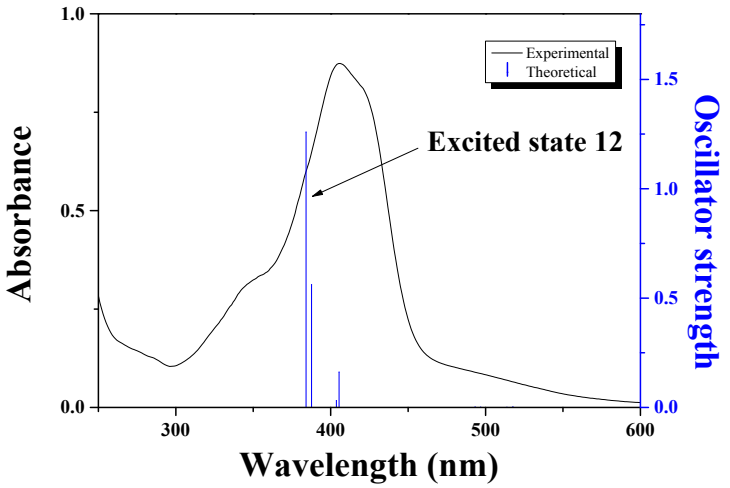

(b)

Excited state 12	Wavelength (nm)	Percent (%)	Main character	Oscillator strength
H-1 → L+3	384.10	76	ICT	1.2591
H → L+2		16	ICT	

Fig. S20 (a) The theoretical excitation energies (TD-DFT method) and the experimental UV-vis spectrum of Ga^{3+}-2·**1** complex. (b) The major electronic transition energies and molecular orbital contributions of Ga^{3+}-2·**1** complex (H = HOMO and L = LUMO).

(a)

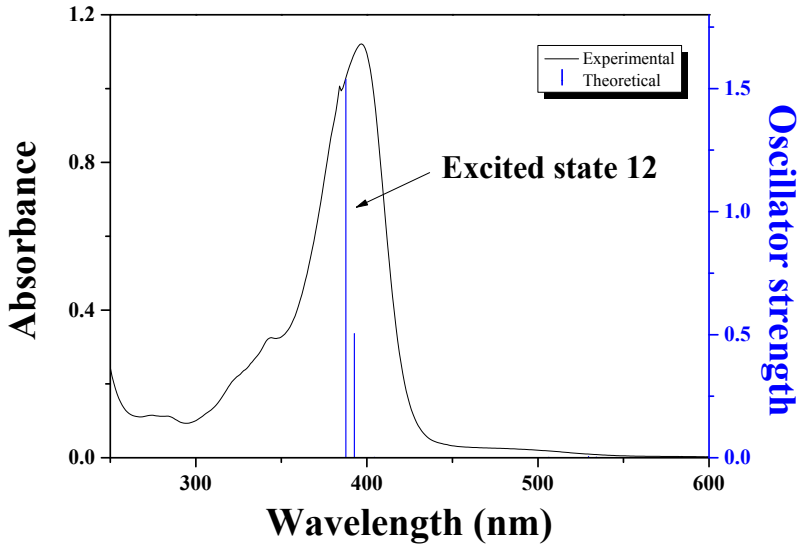

(b)

Excited state 12	Wavelength (nm)	Percent (%)	Main character	Oscillator strength
H-1 → L+2	387.68	43	ICT	1.5361
H → L+3		47	ICT	

Fig. S21 (a) The theoretical excitation energies (TD-DFT method) and the experimental UV-vis spectrum of In^{3+}-2·**1** complex. (b) The major electronic transition energies and molecular orbital contributions of In^{3+}-2·**1** complex (H = HOMO and L = LUMO).

(a)

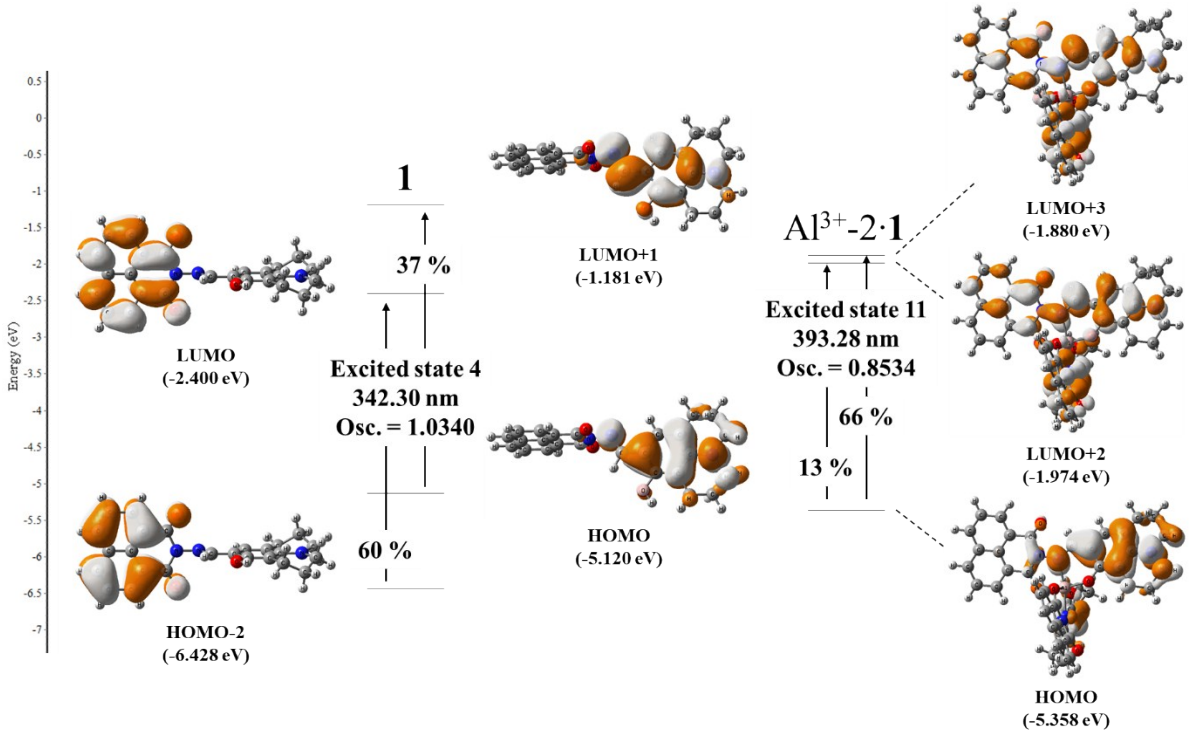
Energy (eV)
1
37 %
Excited state 4
342.30 nm
Osc. = 1.0340
60 %
LUMO
(-2.400 eV)
HOMO-2
(-6.428 eV)
LUMO+1
(-1.181 eV)
HOMO
(-5.120 eV)
Al3+-2·1
Excited state 11
393.28 nm
Osc. = 0.8534
66 %
13 %
LUMO+3
(-1.880 eV)
LUMO+2
(-1.974 eV)
HOMO
(-5.358 eV)

(b)

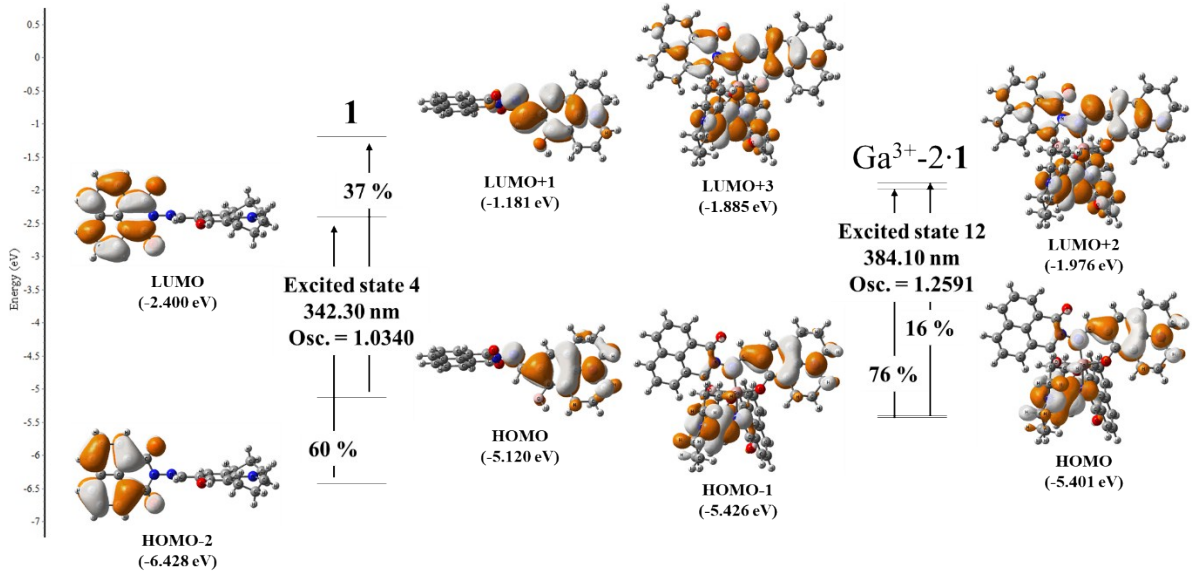
Energy (eV)
1
37 %
Excited state 4
342.30 nm
Osc. = 1.0340
60 %
LUMO
(-2.400 eV)
HOMO-2
(-6.428 eV)
LUMO+1
(-1.181 eV)
HOMO
(-5.120 eV)
LUMO+3
(-1.885 eV)
HOMO-1
(-5.426 eV)
Ga3+-2·1
Excited state 12
384.10 nm
Osc. = 1.2591
16 %
76 %
LUMO+2
(-1.976 eV)
HOMO
(-5.401 eV)

(c)

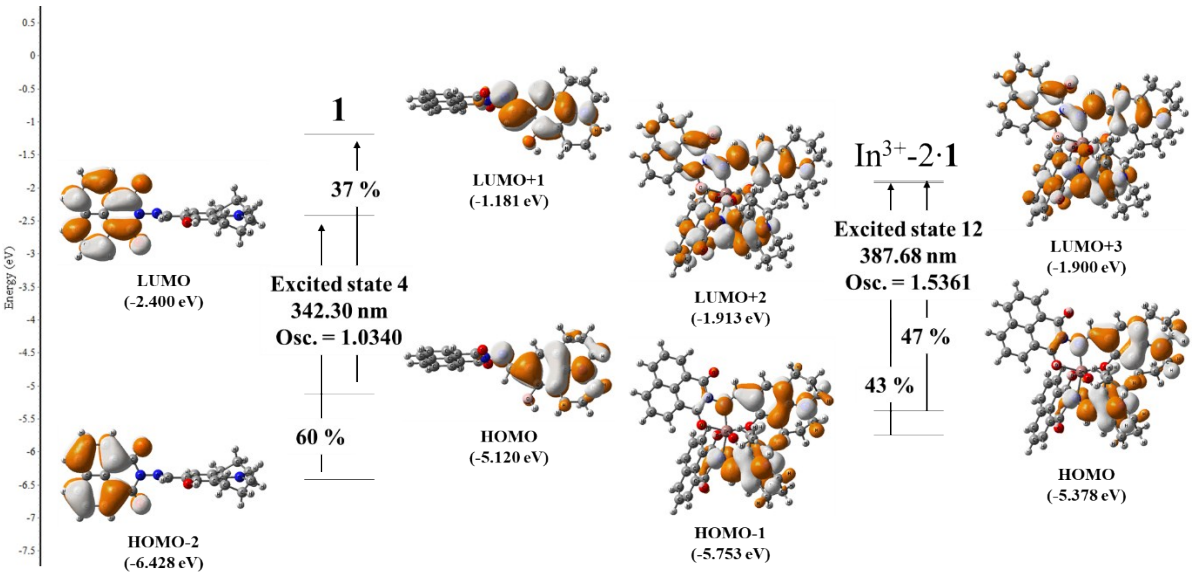

Fig. S22 Molecular orbital diagrams of **1** with (a) Al^{3+}-2·**1**, (b) Ga^{3+}-2·**1** and (c) In^{3+}-2·**1** complexes.